J. Phys. Res. Edu., Vol. 1, March 2024

Spin and valley dependent transport in a biased dice lattice

Lakpa Tamang*

Department of Physics, University of North Bengal, Raja Rammohunpur-734013, India

We study the spin and valley-dependent transport in a spin-orbit coupled biased dice lattice. We find that the presence of a bias term and the spin-orbit interaction (SOI) give rise to the spin-split energy spectrum. The SOI couples the valley and the spin degrees of freedom, resulting in a spin and valley-resolved Berry curvature. We find a profound variation in the Berry curvature for different spin states around both valleys. The spin and valley Hall conductivities are calculated for various values of the bias term. We find the interplay between the bias term and SOI term leads to a quantum phase transition from a topological insulating phase to a trivial band insulating phase accompanied by the emergence of the valley Hall effect and the suppression of the spin Hall effect.

I. INTRODUCTION

Since the discovery of graphene [1], there has been a growing interest in two-dimensional crystals like silicene [2], MoS_2 [3], etc., with a honeycomb lattice structure for potential applications in new-generation electronic devices [4, 5]. The low-energy electrons in such crystals have an extra degree of freedom called "valley". The valley index is associated with the special points of the Brillouin zone, called the Dirac points, K and K' where the energy bands meet each other. Since there is a significant distance in momentum space that separates the valleys, the intervalley scattering is highly suppressed in the presence of smooth scattering potential, thus making valley index an intrinsic property of low energy carriers. Similar to the application of spin in spintronics, the utilization of the valley index for encoding and controlling information leads to the emergence of a new field of research known as valleytronics [6–9]. The valley Hall effect stands out as an intriguing phenomenon resulting from the manipulation of the valley degree of freedom, where a longitudinal electric field drives carriers in opposite transverse directions based on their valley index. D. Xiao [6] first predicted it theoretically in graphene with broken space-inversion symmetry, and subsequently, it was observed experimentally in MoS_2 [10]. The breaking of inversion symmetry in crystals is necessary to manifest valley-contrasting physics. The SOI in such materials couples the valley index with the spin of the carriers, leading to various spin and valley-coupled phenomena. Over the years, various fascinating spin and valley-dependent phenomena like valley polarization by spin [11], spin-valley locking [12, 13], spin-valley interactions [14, 15], spin-valley polarization [16, 17], spin-valley dependent optical selection rules [18], etc, have been extensively studied.

In this paper, we calculate the spin and valley Hall conductivities to study the spin and valley coupled transport properties of a biased dice lattice. To study the effect of the SOI, we consider an intrinsic SOI of Kane-Mele type [19]. The consideration of such SOI usually results in a spin Hall effect [19–21], marked by the emergence of conducting channels along the boundaries of the sample. Our system of interest is a spin-orbit coupled biased dice lattice [22]. The bias term and the SOI break the space-inversion symmetry of the dice lattice. The Dice lattice is a graphene-like two-dimensional material with T_3 symmetry. Like graphene, electrons in the dice lattice obey the Dirac equation near the K and K' points. Although the zero-field spectrum of dice and graphene lattices appears identical, these systems differ fundamentally because the former supports a zero-energy flat band. In the dice lattice, low-energy excitations follow the Dirac-Weyl Hamiltonian with an enlarged pseudospin $S = 1$. Moreover, a significant disparity arises between the graphene and the dice lattice when look at the closed trajectories of the quasiparticles in momentum space. Unlike the Berry phase of π observed in graphene, the quasiparticles in the dice lattice do not acquire any nontrivial Berry phase. Figure 1 illustrates the geometry of the dice lattice, which includes an additional site positioned at the center of each hexagon in the honeycomb lattice connecting with one of the two inequivalent sites of the honeycomb lattice. Among these sites, two (A and C) are referred to as rim sites, while the third (B) is known as a hub site, having coordination numbers of 3 and 6, respectively. Experimental realization of the dice lattice is feasible in a $SrTiO_3/SrIrO_3/SrTiO_3$ heterostructure [23]. Additionally, it can be replicated in an optical lattice [24] setup by confining ultra cold atoms with the aid of three pairs of oppositely moving laser beams.

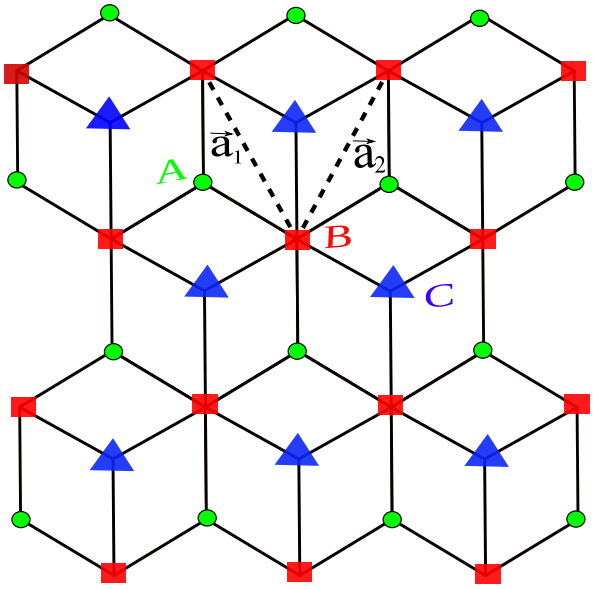

FIG. 1: The lattice geometry of the dice lattice is depicted here, where a_1 and a_2 represent the lattice vectors.

II. MODEL AND METHODS

Allowing the nearest-neighbor (NN) and next nearest-neighbor (NNN) hoppings only, the real space tight-binding Hamiltonian for biased dice lattice can be written as

$$H = t\sum_{\langle ij\rangle}\mathcal{C}_{is}^{\dagger}\mathcal{C}_{js} + t\sum_{\langle jk\rangle}\mathcal{C}_{js}^{\dagger}\mathcal{C}_{ks} + \frac{i\lambda}{3\sqrt{3}}\sum_{\langle\langle ij\rangle\rangle ss'}\mu_{ij}\mathcal{C}_{is}^{\dagger}s_z\mathcal{C}_{js'} + \frac{i\lambda}{3\sqrt{3}}\sum_{\langle\langle jk\rangle\rangle ss'}\mu_{jk}\mathcal{C}_{js}^{\dagger}s_z\mathcal{C}_{ks'} + \sum_{is}\nu_i\Delta_i\mathcal{C}_{is}^{\dagger}\mathcal{C}_{is} \quad (1)$$

where $\mathcal{C}_{is}^{\dagger}(\mathcal{C}_{is})$, $\mathcal{C}_{js}^{\dagger}(\mathcal{C}_{js})$, and $\mathcal{C}_{ks}^{\dagger}(\mathcal{C}_{ks})$ creates (annihilates) an electron of spin polarization s at sites A, B, and C, respectively. The first term in Eq. (1) illustrates the NN hopping between A and B sites, while the next term represents the NN hopping between B and C sites. In both cases the NN hopping strength is t. The third and fourth terms are the Kane-Mele type SOI term arising from the NNN hoppings A-B-A and C-B-C, respectively. Here, λ denotes the strength of the SOI. For clockwise (counter-clockwise) NNN hopping we have $\mu_{ij}, \mu_{jk} = -1\,(+1)$. Here, s, s', and s_z represent the real spin Pauli operators. The final term is the staggered lattice potential or the bias term Δ_i, where ν_i takes $+1$ and -1 for the A and C sites, respectively.

The Hamiltonian in Eq. (1) on projecting into a reciprocal space and expanding it around the Dirac points results in an effective Hamiltonian

$$H(\boldsymbol{k}) = \begin{pmatrix} \Delta - \lambda\tau s & \frac{f_{\boldsymbol{k}}}{\sqrt{2}} & 0 \\ \frac{f_{\boldsymbol{k}}^*}{\sqrt{2}} & 0 & \frac{f_{\boldsymbol{k}}}{\sqrt{2}} \\ 0 & \frac{f_{\boldsymbol{k}}^*}{\sqrt{2}} & -\Delta + \lambda\tau s \end{pmatrix}, \quad (2)$$

where $f_k = \hbar v_F(\tau k_x + ik_y)$ with the Fermi velocity $v_F = 3at/\sqrt{2}$ and $\tau = \pm 1$ is the valley index representing K and K' points. Diagonalizing the Hamiltonian given in Eq. (2), we find the following spin and valley-dependent eigenenergies

$$E_n^{\tau s} = n\sqrt{\epsilon_k^2 + (\Delta - \lambda\tau s)^2}. \quad (3)$$

Here, $n = -1/0/+1$ denotes the valence/flat/conduction band, respectively, and $\epsilon_k = \hbar v_F k$ with $k = \sqrt{(k_x^2 + k_y^2)}$. The presence of the bias term and the SOI term together introduces an energy gap $E_g = |\Delta - \lambda\tau s|$ between the flat band and the conduction band or the valence band at a particular Dirac point.

The corresponding normalized eigenstates are obtained as

$$u_0^{\tau s}(\boldsymbol{k}) = \frac{1}{\sqrt{2}N_0}\begin{pmatrix} \frac{-f_{\boldsymbol{k}}}{(\Delta-\lambda\tau s)} \\ \sqrt{2} \\ \frac{f_{\boldsymbol{k}}^*}{(\Delta-\lambda\tau s)} \end{pmatrix}, u_{\pm1}^{\tau s}(\boldsymbol{k}) = \frac{1}{\sqrt{2}N_{\pm1}}\begin{pmatrix} \frac{f_{\boldsymbol{k}}}{\left(E_{\pm1}^{\tau s}(k)-\Delta+\lambda\tau s\right)} \\ \sqrt{2} \\ \frac{f_{\boldsymbol{k}}^*}{\left(E_{\pm1}^{\tau s}(k)+\Delta-\lambda\tau s\right)} \end{pmatrix}, \tag{4}$$

where $N_0 = \frac{\sqrt{\epsilon_k^2+(\Delta-\lambda\tau s)^2)}}{|\Delta-\lambda\tau s|}$ and $N_{\pm1} = \frac{\sqrt{2}|E_{\pm1}^{\tau s}|}{\epsilon_k}$ are the normalization constants.

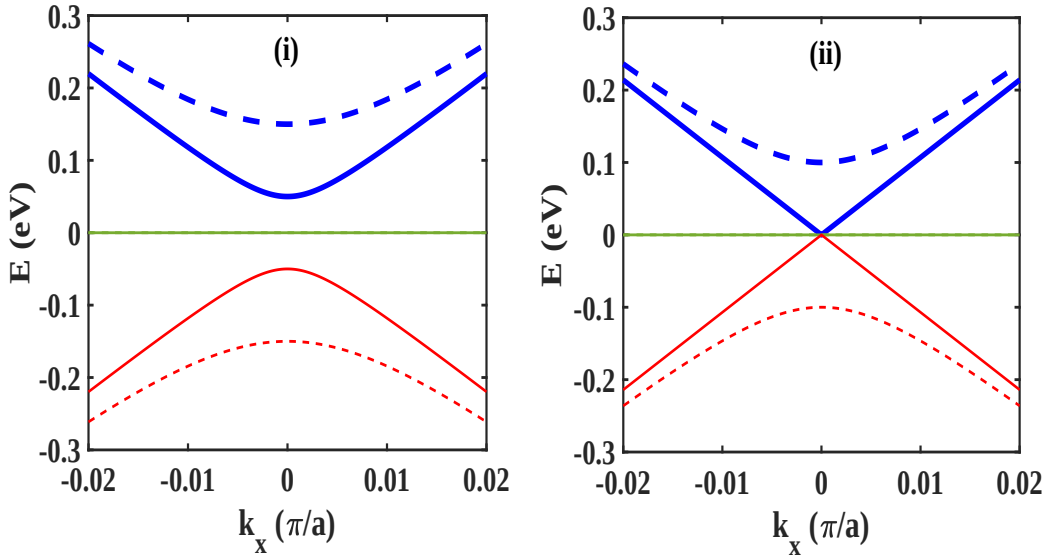

FIG. 2: The energy spectrum of the biased dice lattice for (i) $\Delta \neq \lambda$ and (ii) $\Delta = \lambda$. Thick solid (dashed) line represents the spin-up (spin-down) conduction band (blue in color), thin solid (dashed) line is for the spin-up (spin-down) valence band (red in color) and the Flat green line is the spin degenerate flat band. Here, we have taken $\lambda = 50$ meV.

The broken space-inversion symmetry due to the presence of the bias and the SOI results in a spin and valley-dependent Berry curvature $\Omega_n^{\tau s}(\boldsymbol{k})$. The Berry curvature can be calculated using the relation $\Omega_n^{\tau s}(\boldsymbol{k}) = i\langle\nabla_{\boldsymbol{k}} u_n^{\tau s}(\boldsymbol{k})| \times |\nabla_{\boldsymbol{k}} u_n^{\tau s}(\boldsymbol{k})\rangle$, where $u_n^{\tau s}(\boldsymbol{k})$ is the periodic component of the Bloch function corresponding to the n^{th} energy band. The Berry curvature transforms as $\boldsymbol{\Omega}_n^{\tau s}(\boldsymbol{k}) = \boldsymbol{\Omega}_n^{\tau' s}(\boldsymbol{k})$ and $\boldsymbol{\Omega}_n^{\tau s}(\boldsymbol{k}) = -\boldsymbol{\Omega}_n^{\tau' s'}(\boldsymbol{k})$ under the space-inversion and the time reversal symmetry operations, respectively. Here, $\tau' = -\tau$ and $s' = -s$. Therefore a non-zero Berry curvature demands the breaking of any one of these symmetries.

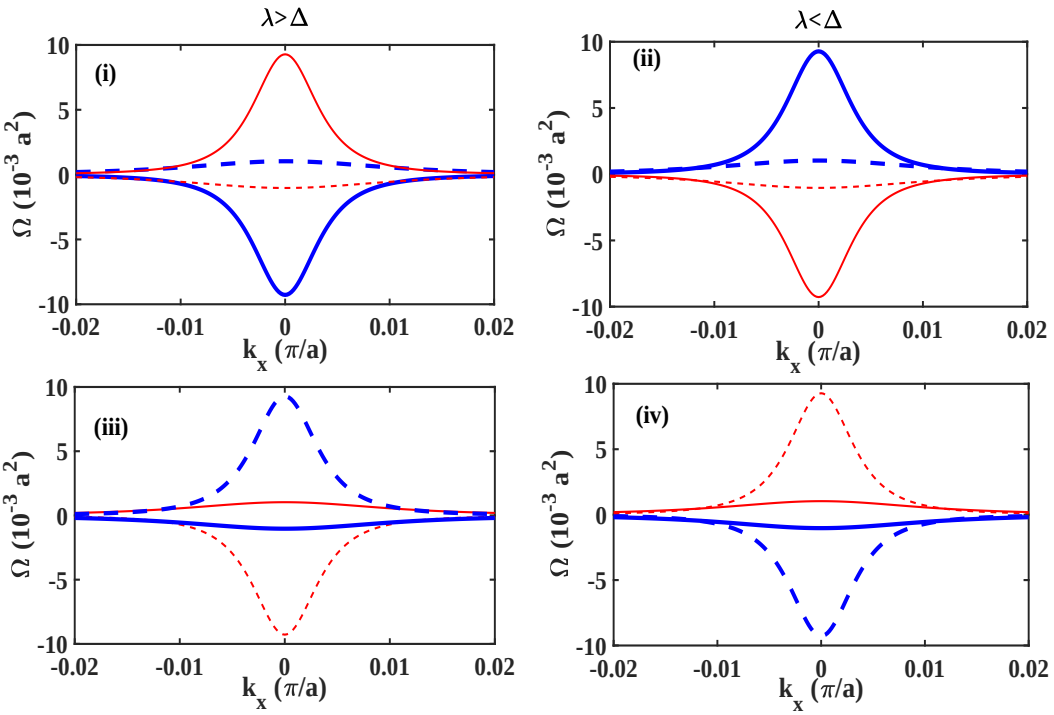

FIG. 3: The variation of Berry curvature around the K valley[(i) and (ii)] and the K' valley[(iii) and (iv)]. The left (right) panel corresponds to $\Delta < \lambda$ ($\Delta > \lambda$). Thick solid (dashed) line indicates the Berry curvature of the spin-up (spin-down) conduction band (blue in color) and thin solid (dashed) line is for the Berry curvature of the spin-up (spin-down) valence band (red in color).

In the presence of an in-plane electric field, $\Omega_n^{\tau s}(\boldsymbol{k})$ imparts an anomalous velocity to an electron perpendicular to its motion, resulting in an intrinsic contribution to the anomalous Hall conductivity [6]

$$\sigma_{xy}^{\tau s} = (e^2/\hbar) \int \frac{d^2\mathbf{k}}{(2\pi)^2} \sum_n f_n(E_n^{\tau s}) \Omega_n^{\tau s}(\boldsymbol{k}), \tag{5}$$

where $f_n(E_n^{\tau s})$ is the Fermi-Dirac distribution function. We define the spin ($\sigma_{xy}^{\text{spin}}$) and valley ($\sigma_{xy}^{\text{valley}}$) Hall conductivities as

$$\sigma_{xy}^{\text{spin}} = \sum_{\tau s} s\sigma_{xy}^{\tau s}, \tag{6}$$

$$\sigma_{xy}^{\text{valley}} = \sum_{\tau s} \tau\sigma_{xy}^{\tau s}. \tag{7}$$

III. RESULTS AND DISCUSSION

The energy spectrum of the biased dice lattice is depicted in Figs. 2 for K valley. There are, in principle, six energy bands, three associated with spin-up and three with spin-down electrons. Here, we treat λ as a fixed parameter and assume that Δ is a freely adjustable parameter. We have plotted the energy spectrum for $\lambda \neq \Delta$ and $\lambda = \Delta$ cases. In Fig. 2(i), when $\lambda \neq \Delta$ ($\lambda = 100$ meV, $\Delta = 50$ meV), we observe a splitting of the conduction and valence bands, resulting in a finite gap between both spin-up and spin-down bands. Conversely, when $\Delta = \lambda = 50$ meV, Fig. 2(ii) demonstrates a gapless Dirac cone for the spin-up electrons and a gapped Dirac cone for the spin-down electrons. This state has been termed a valley-spin-polarized metal (VSPM) [25]. In this case, electrons with only one spin polarization are significant for device applications facilitating spin-polarized transport. However, the flat band is nondispersive and spin degenerate in both cases. Because of the time-reversal symmetry, the spin splitting in the two valleys exhibits an opposite behavior. The role played by spin-up bands in the K valley is mirrored by spin-down bands in the K' valley. Using Eq. (4), we find the Berry curvature for the individual band analytically as

$$\Omega_{\pm}^{\tau s}(\boldsymbol{k}) = \mp\tau \frac{\hbar^2 v_F^2(\Delta - \lambda\tau s)}{[\epsilon_k^2 + (\Delta - \lambda\tau s)^2]^{3/2}} \text{ and } \Omega_0^{\tau s}(\boldsymbol{k}) = 0. \tag{8}$$

The Berry curvature associated with the conduction and valence bands are equal in magnitude but opposite in sign as a consequence of the particle-hole symmetry. However, Berry curvature of the flat band vanishes due to its nondispersive nature. Furthermore, with the inclusion of the bias and the SOI terms, the Berry curvature becomes spin and valley resolved. Figures 3(i) and 3(iii) depict the Berry curvature of conduction and valence bands for $\lambda > \Delta$ around K and K' valleys, respectively. The distribution of Berry curvatures is mainly centered around $\boldsymbol{k}$=0. In the K valley, for spin-up states, the Berry curvature of the conduction band is negative, and that of the valence band is positive. Conversely, its sign reverses with reduced magnitude for the spin-down states. However, in the K' valley, the Berry curvature follows the relation $\boldsymbol{\Omega}_n^{\tau s}(\boldsymbol{k}) = -\boldsymbol{\Omega}_n^{\tau' s'}(\boldsymbol{k})$ as a consequence of the time-reversal symmetry. The variation of the Berry curvature for $\lambda < \Delta$ around K and K' valleys is depicted in Figs. 3(ii) and 3(iv), respectively. In this case, the Berry curvature for spin-up states exhibits an opposite trend, while that for spin-down states remains consistent with the observations made when $\lambda > \Delta$. The pronounced variation observed in the Berry curvature for different spin states around both the valleys emphasizes the potential for manipulating spin and valley characteristics of the Berry curvature.

Using Eqs. (5) and (8), we calculate the analytical expression of Hall conductivity at zero temperature for various positions of the chemical potential (μ). For μ in the band gap, we obtain

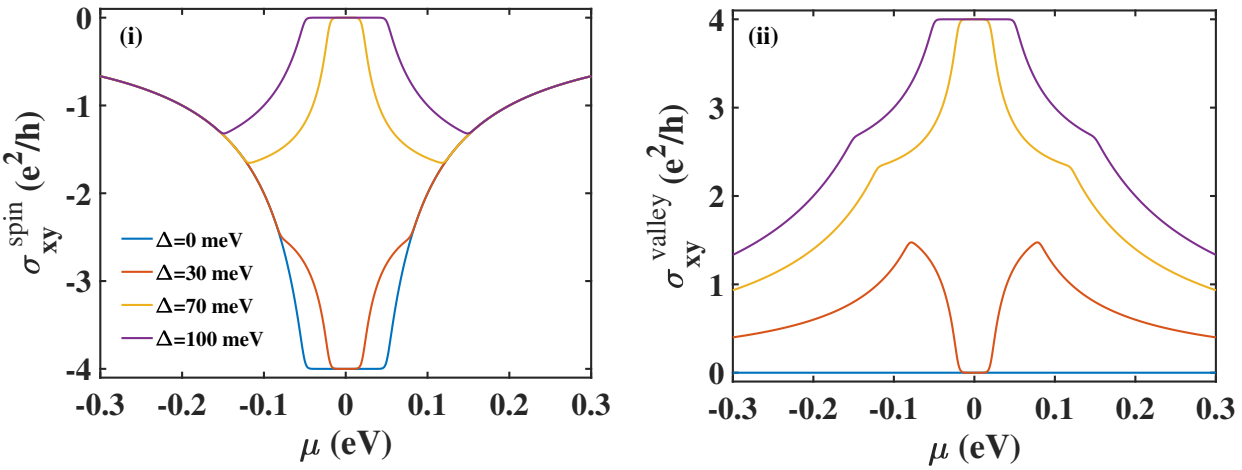

FIG. 4: The variation of (i) Spin and (ii) Valley Hall conductivities with the chemical potential (μ) for different values of Δ at $T = 20$K. Here we have considered $\lambda = 50$ meV.

$$\sigma_{xy}^{\tau s} = \tau \frac{e^2}{h} \frac{(\Delta - \lambda \tau s)}{|\Delta - \lambda \tau s|}. \tag{9}$$

Using Eqs. (6) and (7), we obtain the analytical expressions of $\sigma_{xy}^{\text{spin}}$ and $\sigma_{xy}^{\text{valley}}$ as

$$\sigma_{xy}^{\text{spin/valley}} = 2\frac{e^2}{h}\Big[\text{sgn}(\Delta - \lambda) \mp \text{sgn}(\Delta + \lambda)\Big], \tag{10}$$

where the $-(+)$ sign denotes the spin (valley) Hall conductivity. The interplay between Δ and λ leads to various phases, which can be characterized based on the values of $\sigma_{xy}^{\text{spin}}$ and $\sigma_{xy}^{\text{valley}}$ as

$$\sigma_{xy}^{\text{spin}} = \frac{e^2}{h} \begin{cases} -4 & \Delta < \lambda \\ -2 & \Delta = \lambda \\ 0 & \Delta > \lambda \end{cases}$$

and

$$\sigma_{xy}^{\text{valley}} = \frac{e^2}{h} \begin{cases} 0 & \Delta < \lambda \\ 2 & \Delta = \lambda \\ 4 & \Delta > \lambda. \end{cases}$$

When μ lies in the band gap, both $\sigma_{xy}^{\text{spin}}$ and $\sigma_{xy}^{\text{valley}}$ take a quantized values. For $\Delta < \lambda$, we have a finite $\sigma_{xy}^{\text{spin}}$ with vanishing $\sigma_{xy}^{\text{valley}}$, indicative of a topological insulator or Quantum spin Hall insulator phase [19],

with conductive channels at the boundary of the system. When $\Delta = \lambda$, both $\sigma_{xy}^{\text{spin}}$ and $\sigma_{xy}^{\text{valley}}$ simultaneously acquire non-zero values, indicating a VSPM phase [25]. A trivial insulator phase [6] emerges for $\Delta > \lambda$ with vanishing $\sigma_{xy}^{\text{spin}}$ and a finite $\sigma_{xy}^{\text{valley}}$.

When μ lies in the conduction band, we obtain

$$\sigma_{xy}^{\tau s} = \tau \frac{e^2}{h} \left[\frac{(\Delta - \lambda \tau s)}{E_F} \right], \tag{11}$$

where $E_F = \sqrt{\hbar^2 v_F^2 k_F^2 + (\Delta - \lambda \tau s)^2}$. The corresponding $\sigma_{xy}^{\text{spin}}$ and $\sigma_{xy}^{\text{valley}}$ are calculated as

$$\sigma_{xy}^{\text{spin/valley}} = 2 \frac{e^2}{h} \Big[\frac{(\Delta - \lambda)}{E_F} \mp \frac{(\Delta + \lambda)}{E_F} \Big]. \tag{12}$$

Here the $-(+)$ sign corresponds to the spin (valley) Hall conductivity. Due to the particle-hole symmetry, a similar expression can be obtained when μ lies in the valence band. The variation of $\sigma_{xy}^{\text{spin}}$ as a function of μ for different values of the parameter Δ is depicted in Fig. 4(i). Within a band gap, $\sigma_{xy}^{\text{spin}}$ takes a quantized and finite value as long as $\Delta < \lambda$ and vanishes for $\Delta > \lambda$, indicating a transition from a topological insulator to a trivial insulator phase. Additionally, it is observed that the width of the Hall plateau diminishes as Δ increases, suggesting a reduction in the width of a band gap. The behavior of $\sigma_{xy}^{\text{valley}}$ as a function of μ with increasing values of Δ is shown in Fig. 4(ii). For $\Delta = 0$, $\sigma_{xy}^{\text{valley}}$ vanishes for all values of μ, implying the necessity of a non-zero value of the bias term to break the valley degeneracy and observe the valley Hall effect. As Δ increases, for $\Delta < \lambda$, $\sigma_{xy}^{\text{valley}}$ remains zero within a band gap, while for $\Delta > \lambda$, it takes a quantized and finite value.

IV. CONCLUSION

In summary, we have investigated the spin and valley-dependent transport in the biased dice lattice. The presence of the bias and the SOI terms leads to a spin-split energy band structure. However, the flat band remains spin degenerate. We have obtained analytical expressions of the Berry curvature corresponding to individual bands. We analyzed the variations of the spin and valley Hall conductivities as a function of the chemical potential analytically and numerically. It is observed that the interplay between the bias and the SOI terms leads to a quantum phase transition from a topological insulator phase to a trivial insulator phase. This phase transition can be characterized by the appearance of the valley Hall effect and the suppression of the spin Hall effect, indicating a profound impact of the interplay of the bias and the SOI terms on the transport properties of the system. Our results could provide valuable insights for developing spintronics and valleytronics devices.

ACKNOWLEDGMENTS

The author sincerely acknowledges Dr. Tutul Biswas for his valuable suggestions.

* Electronic address: lakpatamang@nbu.ac.in

[1] K. S. Novoselov *et al*, Science **306**, 666 (2004).

[2] P. Vogt *et al*, Phys. Rev. Lett. **108**, 155501 (2012).

[3] D. Xiao, G-B. Liu, W. Feng, X. Xu, and W. Yao, Phys. Rev. Lett.**108**, 196802 (2012).

[4] K. S. Novoselov *et al*, Proc. Natl. Acad. Sci. **102**, 10 451 (2005).

[5] C. Lee, Q. Li, W. Kalb, X.-Z. Liu, H. Berger, R. W. Carpick, and J. Hone, Science **328**, 76 (2010).

[6] D. Xiao, W. Yao, Q. Niu, Phys. Rev. Lett. **99**, 236809 (2007).

[7] A. Rycerz, J. Tworzydlo, and C. W. J. Beenakker, Nat. Phys. **3**, 172 (2007).

[8] M. Ezawa, Phys. Rev. Lett. **110**, 026603 (2013).

[9] Z. P. Niu and S. Dong, Appl. Phys. Lett. **104**, 202401 (2014).

[10] K. F. Mak, K. L. McGill, J. Park, and P. L. McEuen, Science **344**, 1489 (2014).

[11] O. L. Sanchez, D. Ovchinnikov, S. Misra, A. Allain, and A. Kis, Nano Lett. **16**, 5792 (2016).

[12] L. Bawden *et al*, Nat Commun **7**, 11711 (2016).

[13] J.Y. Liu *et al*, Nat Commun **12**, 4062 (2021).

[14] R. Pisoni *et al*, Phys. Rev. Lett. **121**, 247701 (2018).

[15] N. Stefanidis and I. S. Villadiego, Phys. Rev. B **108**, 235137 (2023).

[16] J-T. Sun *et al*, 2D Mater. **3**, 035026, (2016).

[17] T. Zhou *et al*, npj Quant Mater **3**, 39 (2018).

[18] M. Ezawa, Phys. Rev. B **86**, 161407(R) (2012).

[19] C. L. Kane and E. J. Mele, Phys. Rev. Lett. **95**, 226801 (2005).

[20] C. L. Kane and E. J. Mele, Phys. Rev. Lett. **95**, 146802 (2005).

[21] C-C. Liu, W. Feng, and Y. Yao, Phys. Rev. Lett. **107**, 076802 (2011).

[22] L. Hao, Phys. Rev. B **104**, 195155 (2021).

[23] F. Wang, Y. Ran, Phys.Rev. B. **84**, 241103 (2011).

[24] M. Rizzi, V. Cataudella, and R. Fazio, Phys. Rev. B **73**, 144511 (2006).

[25] M. Ezawa, Phys. Rev. Lett. **109**, 055502 (2012).

